Application of 3D laser scanning in monitoring of a barren slope

Tsung-Chiang Wu, National Chung-Hsing University, Taichung, Taiwan
Zheng-Yi Feng, National Chung-Hsing University, Taichung, Taiwan
Wen-Fu Chen, National Chung-Hsing University, Taichung, Taiwan

Abstract

This study utilizes the 3D scanning technology to obtain high accuracy 3D point-cloud coordinates for a barren slope area. The data of point-clouds were scanned twice on two different dates to analyze the changes and deformations of the slope for its range, size and locations. This method can measure the 3D slope surface accurately, and improve the accuracy of comparison between the two measurements. After the proposed post-process procedures, this study shows that 3D laser scanning technology is very useful in monitoring barren slope for its movement, changes, sliding volume, etc. Further applications for slope/landslides should include understanding long-term creep tendency, detection of the extent of landslide and prediction/warning of future sliding.

1. Introduction

Under Taiwan's special climate conditions, intense rainfalls always trigger landslides during long typhoon season in summer. When there are residents/facilities close to the landslide areas, actions are often taken to reduce the risks due to the landslides. More often than not there could be no long enough timeslot for us to perform mitigation work immediately, the landslide area may keep enlarging and continue to deform. In order to better understand the activity of a landslide, monitoring approaches are often suggested. However, traditional landslide monitoring uses surveying, physical measurement equipments (such as inclinemeter) and/or accurate measurement method (such as accurate Global Positioning System, GPS) to detect activities of landslides. The monitoring work is always time consuming and the data are not enough for a comprehensive terrain changing analysis. Further, if the landslide area is inaccessible (or of dangerous), only a very limited topographical data can be obtained. Mitigation decision of the landslide will be delayed or affected.

Therefore, this study is aiming at developing a continuous monitoring and analyzing

approaches for barren slope/landslide areas using advanced 3D laser scanning (ground-based Light Detection And Ranging, LiDAR). The 3D laser scanner was utilized to obtain a large amount of accurate 3D coordinates of a slope for representing its terrain topography. Also, the technique was applied for analyzing of the terrain changes and deformation of the sliding area, including calculation of the volumes of accumulation and depletion zones that occurred during a 45-day period. Recommendations are also given for handling of possible error sources during data interpretations.

2. Research methodology

A slope after mining near Mountain Pillow in Taiwan was selected for the study (Fig. 1). The 3D scanner was used to measure the first point-cloud data set of the slope surface. After 45 days, the scanner was used again to obtain the second data set. The two sets of data were analyzed for slopes changes. The two sets of data were compared by matching the coordinates of the fixed “conjugate scanning spheres” (Fig. 3) and transforming the coordinate systems of different scanning stations. The method and principle are described as following.

Fig. 1 A slope after mining near Mountain Pillow in Taiwan

2.1 3D laser scanning technology and processing method

“Time of flight” scanning principle of 3D laser scanner is used to calculate the distance (ρ) in EQ.2.1 between the scanner and the object (Fig. 2) using speed of light (c) and the travel time ($\triangle t$). Impulse laser light is produced form the diode of the scanner and the signal reflected back from the surface of the object will be received.

$$\rho = \frac{1}{2} c\Delta t \quad \text{.....EQ.2.1}$$

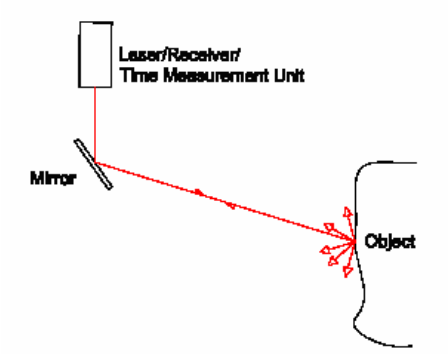

Fig. 2 Time of flight（Boehler, 2001）

We need to first set up the 3D laser scanner in a proper scanning station nearby the landslide slope. The scanning station is required to be set within the effective scanning distance of the scanner. For this case, it is 200 meters between the scanner and the objects to be scanned. At least three conjugate scanning spheres should be installed for matching process.

Fig.3 Scanning station and the 3D scanner (left) and one of the conjugate scanning spheres (right).

2.2 Coordinate system transformation of different scanning stations

The two scanning operations used two different scanning stations. When overlapping the two scanned data sets, we choose the first scanning station to be the “base” coordinate system, and the coordinate system of second scanning station is transformed to the base coordinate system. The conjugate scanning spheres will be the common (matching) points of the two sets of scanned data. Fig. 4 shows the spatial coordinate relationship between the scanning stations and a conjugate scanning sphere. S is the position of the second laser scanner. P is the position of a conjugate scanning sphere. O is the position of the “base” laser scanner (base

coordinate system). ρ is the distance from S to P. α is the plunge angle of SP referring to the xy-plane of the second coordinate system, and θ is the angle between the projection line of SP on the xy-plane and x-axis of the second coordinate system.

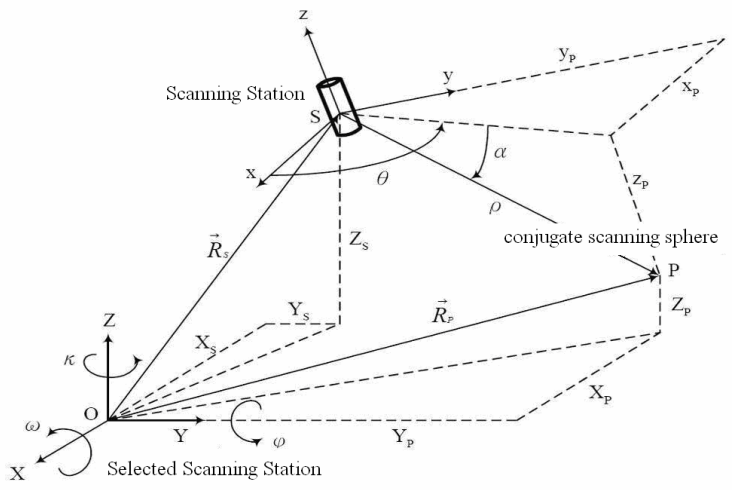

Fig. 4 The spatial coordinate relationship between scanning stations and conjugate scanning spheres（modified from Lichti, 2002）

The mathematic formula of the coordinate system of second scanning station transformed to the base coordinate system is shown as in EQ.2.2. The coordinates of the three or more conjugate scanning spheres are used for coordinate matching and transformation.

$$\vec{R}_p = M\vec{r}_p + \vec{R}_s \quad \text{.....EQ.2.2}$$

where, $\vec{r_p} = \begin{bmatrix} x_p & y_p & z_p \end{bmatrix}^T$: the vector coordinate of conjugate spheres in base coordinate system;

$\vec{R_p} = \begin{bmatrix} X_p & Y_p & Z_p \end{bmatrix}^T$: the vector coordinate of conjugate spheres in the second coordinate system;

$\vec{R_s} = \begin{bmatrix} X_s & Y_s & Z_s \end{bmatrix}^T$: the vector coordinate of the second coordinate system after transformed into the base coordinate system;

M is the rotation matrix of X-, Y-, Z-axis and the angles (ω, φ, κ).

$$M = \begin{bmatrix} \cos\phi\cos\kappa & \cos\omega\sin\kappa + sin\omega\sin\phi\cos\kappa & \sin\omega\sin\kappa - \cos\omega\sin\phi\cos\kappa \\ -\cos\phi\sin\kappa & \cos\omega\cos\kappa - sin\omega\sin\phi\sin\kappa & \sin\omega\cos\kappa + \cos\omega\sin\phi\sin\kappa \\ \sin\phi & -\sin\omega\cos\phi & \cos\omega\cos\phi \end{bmatrix}$$

2-3 The approach of overlapping analysis for terrain changes and deformation

The purpose of overlapping analysis of the two sets of 3D point-cloud data is to calculate for terrain changes and deformation. After the second set of the data has been transformed to the base coordinate system using the method introduced in previous section, the difference of the surface changes/variations between the two sets of data can be calculated using the procedures proposed below.

(a) Using Triangulated Irregular Network (TIN) to build a surface from a set of irregularly spaced points for each set of the two scanned point-cloud data (Fig. 5).

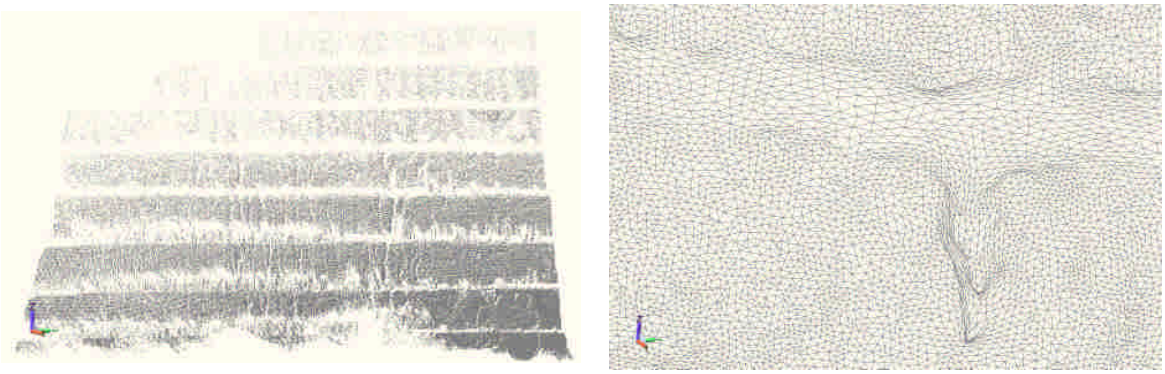

Fig. 5 The 3D point-cloud data (left); the surface model composed using TIN (right).

(b) Importing the two TIN surface models to a same coordinate system, then calculate the vertical difference distances between the two TIN surfaces. It is done by finding the coordinates of all the vertices of the triangles of first TIN surface, then extending vertical lines in Z-axis direction from the vertices to intercept the second TIN surface as shown in Fig.6, and locating the coordinates of the interception points. 6; finally, calculating the vertical difference distance (ΔZ_n) between the vertex and the interception point. We consider that a ΔZ_n value is the variation amount at a single point of the first scanning.

In a TIN surface model, the planar equation for a triangle is:

$AX + BY + CZ + D = 0$.

The three vertices of a triangle are: I (X_1, Y_1, Z_1) 、J (X_2, Y_2, Z_2) 、K (X_3, Y_3, Z_3) . Therefore,

$$A=\begin{bmatrix}Y_1\\Y_2\\Y_3\end{bmatrix}^T\begin{bmatrix}(Z_2-Z_3)\\(Z_1-Z_3)\\(Z_2-Z_1)\end{bmatrix},\ B=\begin{bmatrix}Z_1\\Z_2\\Z_3\end{bmatrix}^T\begin{bmatrix}(X_2-X_3)\\(X_1-X_3)\\(X_2-X_1)\end{bmatrix},\ C=\begin{bmatrix}X_1\\X_2\\X_3\end{bmatrix}^T\begin{bmatrix}(Y_2-Y_3)\\(Y_1-Y_3)\\(Y_2-Y_1)\end{bmatrix}$$, and

$$D=-AX_1-BY_1-CZ_1.$$

On any triangle, $Z=-\frac{A}{C}X-\frac{B}{C}Y-\frac{D}{C}$ EQ.2.3

Assume that $P(a_1,b_1,c_1)$ and $Q(a_2,b_2,c_2)$ are two points in space, then the line equation passing through Point P and Q in space is:

$$L:\begin{Bmatrix}X=a_1+(a_2-a_1)t\\Y=b_1+(b_2-b_1)t\\Z=c_1+(c_2-c_1)t\end{Bmatrix},t\in R\}.$$

If the line L parallel to Z-axis, then $a_1=a_2, b_1=b_2$; therefore,

$$L:\begin{Bmatrix}X=a_1\\Y=b_1\\Z=c_1+(c_2-c_1)t\end{Bmatrix},t\in R\}.$$

Assume $D(X_d,Y_d,Z_d)$ is a point on the spatial line L, then the distance from Point D to the interception point $E(X_e,Y_e,Z_e)$ is:

$$S=\left|Z_e-Z_d\right|\quad,\quad Z_e=-\frac{A}{C}X_d-\frac{B}{C}Y_d-\frac{D}{C}$$ EQ.2.4

The *S* in EQ.2.4 is the difference between the two TIN surface models (Fig.6). If $Z_e-Z_d>0$, the ground surface is accumulating. If $Z_e-Z_d=0$, ground surface is no change. If $Z_e-Z_d<0$, the ground surface is depleting.

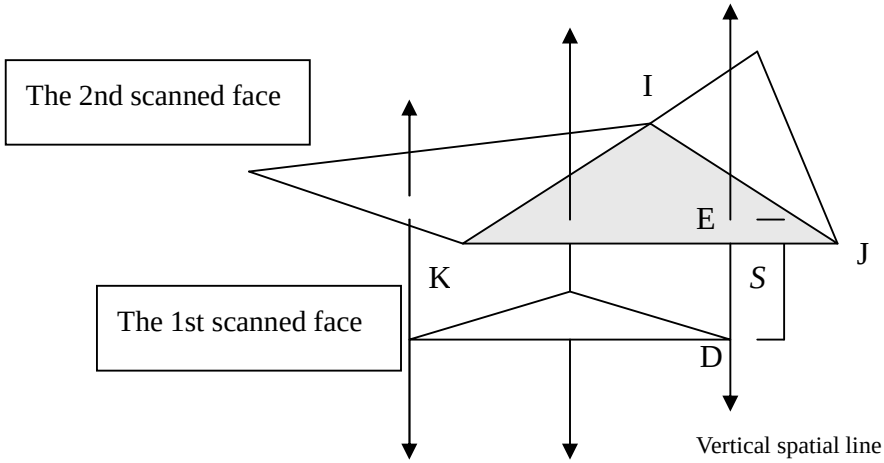

Fig. 6 Vertical difference distances between the two TIN surfaces (referring to the 1st scanned face)

2.4 Flowchart of the approaches (Fig. 7)

The approaches of handling the scanned data for the study introduced in Section 2 are summarized in Fig. 7. The data processing results of the approaches are shown in Section 3.

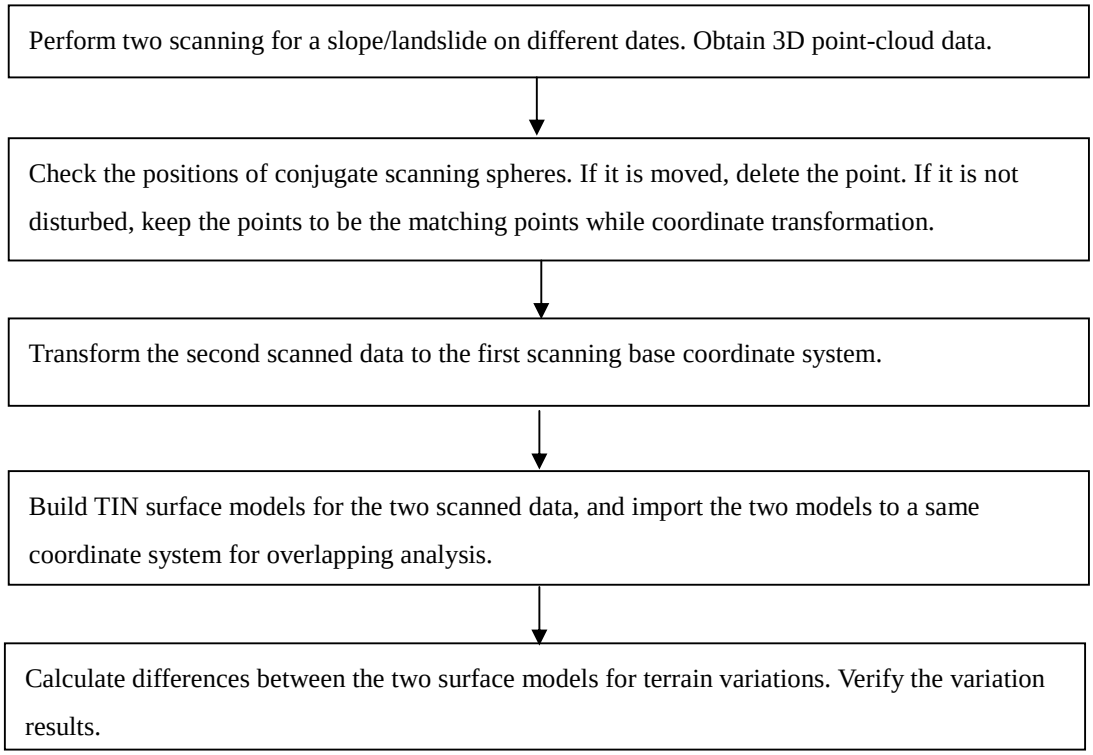

Fig.7 Flowchart of the approaches

3. Data processing

3.1 Perform two scanning for a slope/landslide on different dates. Obtain 3D point-cloud data.

The 3D point-cloud data from the two scanning operations are shown in Fig. 8.

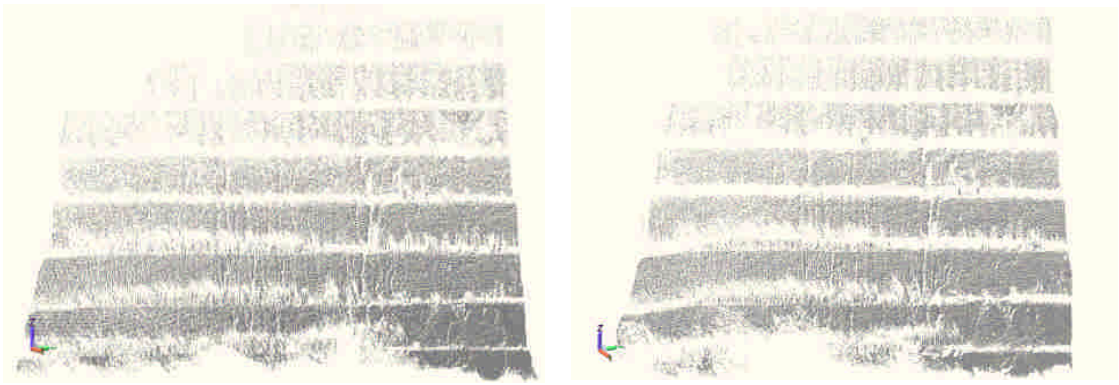

Fig. 8 3D point-cloud data from the first scanning (left) and the second scanning (right)

Table1 Distances back-calculated between conjugate scanning spheres for the two scanning operations (unit: mm)

Distance (conjugate sphere to conjugate sphere)	Distance back-calculated from the first scanning coordinate	Distance back-calculated from the second scanning coordinate	Distance error	Distance error/distance, (**accuracy**)
d01-d02	6090.07	6084.71	-5.36	1/1135.68, (1135.68)
d01-d03	3247.27	3241.61	-5.66	1/573.91, (573.91)
d01-d04	5267.73	5255.42	-12.31	1/427.88,(427.88)
d02-d03	7060.47	7059.42	-1.06	1/6674.47,(6674.47)
d02-d04	3184.85	3183.72	-1.13	1/2820.60,(2820.60)
d03-d04	4698.10	4693.85	-4.25	1/1104.59,(1104.59)

3.2 Check the positions of conjugate scanning spheres. If it is moved, delete the point. If it is not disturbed, keep the points to be the matching points while coordinate transformation.

The distances back-calculated between conjugate scanning spheres (d01, d02, d03, d04) for the two scanning operations are listed in Table 1. As shown in Table 1, the distance accuracy of d01-d03 and d01-d04 are smaller than 1000; the others are all larger than 1000. It means that the conjugate sphere d01 may had been tempered during the two scanning operations.

Therefore, we should delete d01 from being matching point, and use d02, d03, d04 as the common points for further matching calculations.

3.3 Transform the second scanned data to the first scanned base coordinate system.

Table 2 presents the results of transforming the second scanning coordinate of conjugate scanning sphere to the base coordinate system. It also shows that the maximum error is 7.34mm, and the minimum error is -0.01mm.

Table2 Coordinates of the conjugate scanning spheres transformed to the base coordinate system (unit: mm)

Conjugate sphere	First scanning (base) coordinate system（E1）			Second scanning coordinate system （E2）		
	X	Y	Z	X	Y	Z
d02	3180.93	-11304.39	-1738.54	-13286.04	113.27	-1842.69
d03	7770.54	-16652.16	-2171.14	-19880.49	-2364.72	-2299.04
d04	3626.09	-14451.34	-1942.97	-16393.86	768.82	-2061.49
Conjugate sphere	E2 transformed to E1			Error of transform		
	X	Y	Z	X	Y	Z
d02	3183.03	-11304.27	-1738.62	2.10	0.12	-0.08
d03	7772.93	-16650.40	-2171.15	2.39	1.76	-0.01
d04	3633.43	-14449.33	-1943.07	7.34	2.01	-0.10

3.4 Build TIN surface models for the two scanned data, and import the two models to a same coordinate system for overlapping analysis.

The two sets of point-cloud data were used to build TIN surface models as shown in Fig. 9 and Fig.10. Overlapping of the two sets of point-cloud data and TIN models are shown in Fig.11.

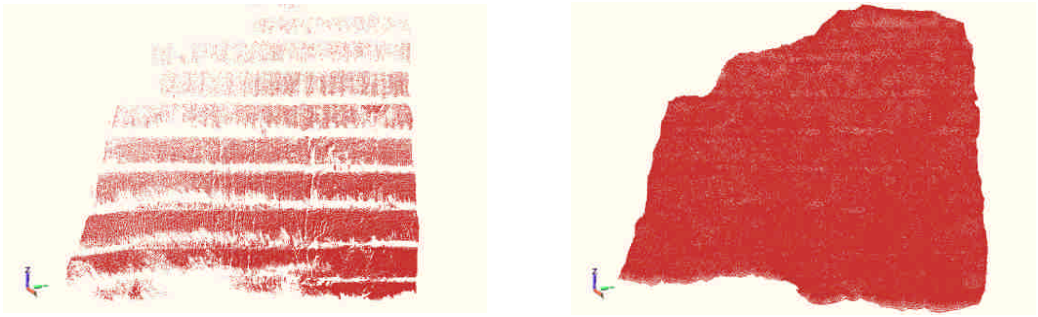

Fig. 9 The first scanning point-cloud data (left) and TIN model (right)

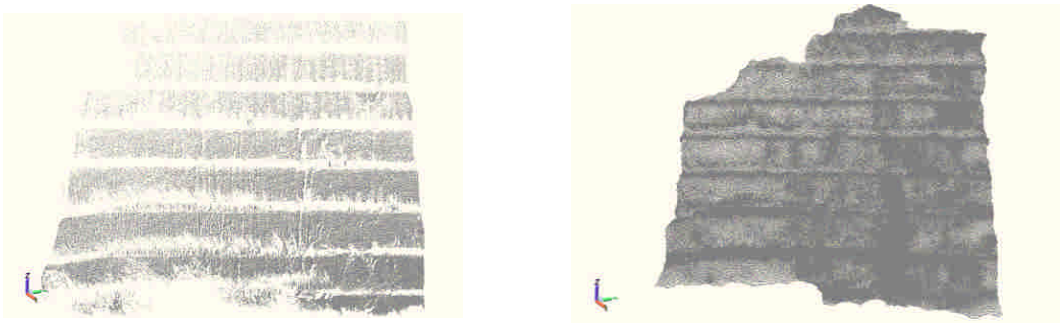

Fig. 10 The second scanning point-cloud data (left) and TIN model (right)

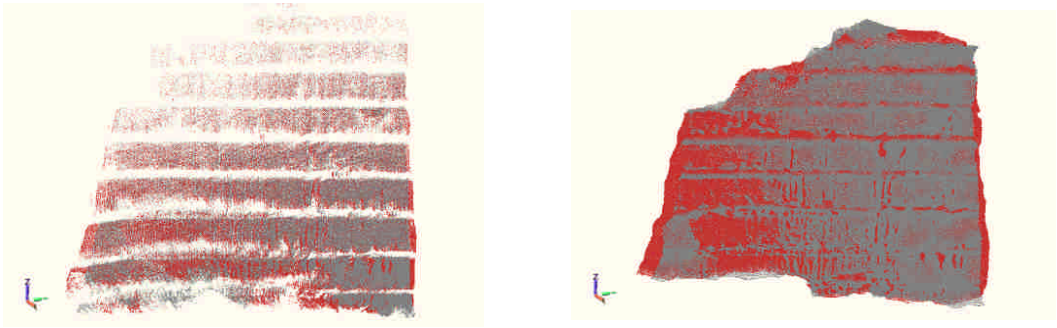

Fig. 11 Overlapping of the two sets of point-cloud data (left) and TIN models (right).

3.5 Calculate differences between the two surface models for terrain variations.

Enlarged TIN models are shown in Fig. 12. The difference (surface changes) between the two scanning surfaces can be calculated using the method introduced in Section 2.3. The differences of each vertex can be used for interpolation in TIN model to show the surface variations using various colors as shown in Fig.13.

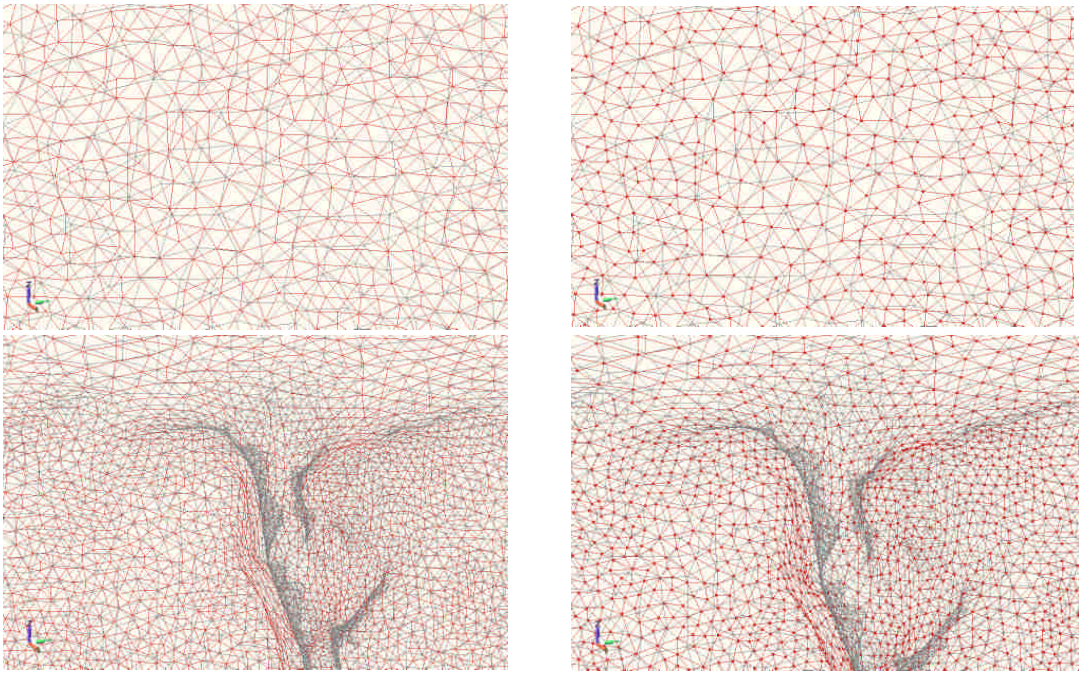

Fig. 12 Overlapping TIN model for a flat zone (upper left); vertices of triangles of the first scanning TIN surface for a flat zone (upper right); Overlapping TIN model for a undulate zone (lower left); vertices of triangles of the first scanning TIN surface for a undulate zone (lower right). Note: The first scanning TIN is shown in red color, and the second scanning TIN in grey.

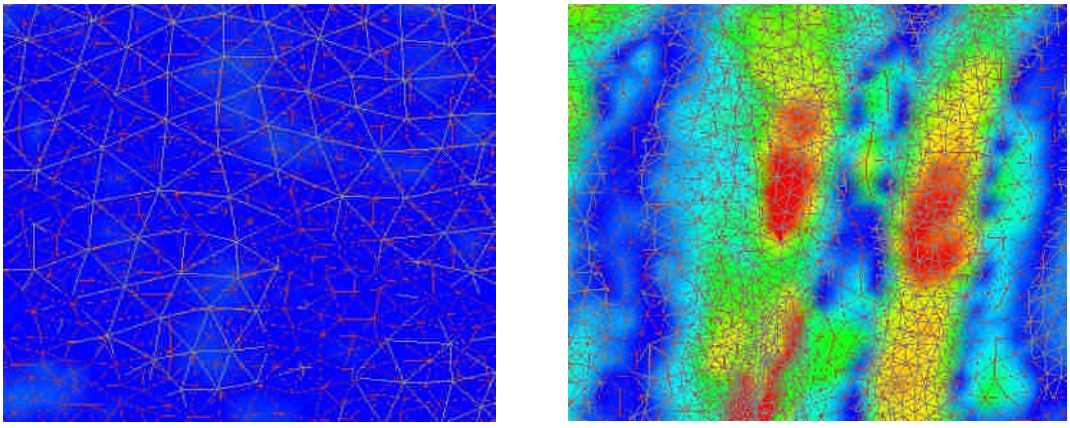

Fig. 13 Surface variations of a flat zone (left); Surface variations of a undulate zone shown by various colors (right).

4. Result discussions

The surface variation result after data processing is shown in Fig. 14. The dark blue color is where no variation occurs. They are evenly distributed and consisting with in-situ condition. The non- dark blue parts are the variation zones. It also fits the in-situ changes very well. While scanning, some surfaces may be blocked due to terrain, obstacles and scanning angle. Therefore, no point-cloud data for those surfaces can be obtained. For example, the red rectangle area in Fig. 14 (also refer to Fig. 8). During data processing, the no-data areas have to be assumed values by interpolation.

The variations shown in the black rectangle areas in Fig. 14 are due to weeds growing on the slope surface during the two scanning dates. To prevent misjudgment on surface variation, the changes and deformation should be verified with site photos as shown in Fig. 15.

There are some green color (and some red color) areas in Fig. 14. The areas are mostly surface cracks or larger undulate areas and they are not surface variation. This could be due to the two scanning stations were not set at a same location. Some discrepancies in interpolation for blocked surface could be generated. Therefore, we suggest installation of a fixed base-plate for scanning station to maintain a same scanning location.

For the red color areas in Fig. 14, it is where the variations are greater than 40cm. It can be a local sliding. The yellow rectangle area as shown in Fig. 14 is the sliding area identified by this study and can be compared to the site photo as shown in Fig.16.

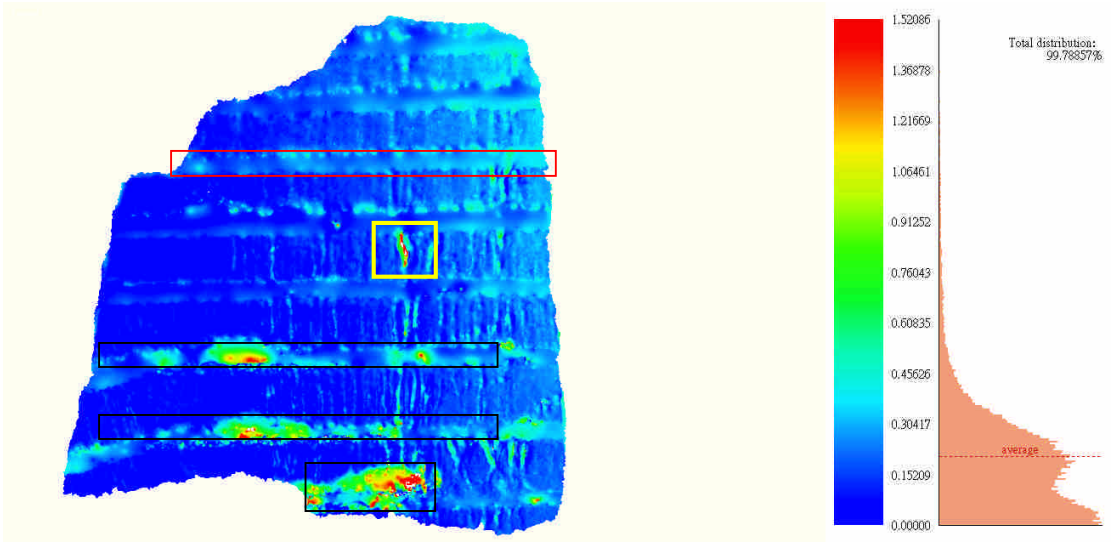

Fig. 14 The surface variation result after overlapping the two scanned data sets.

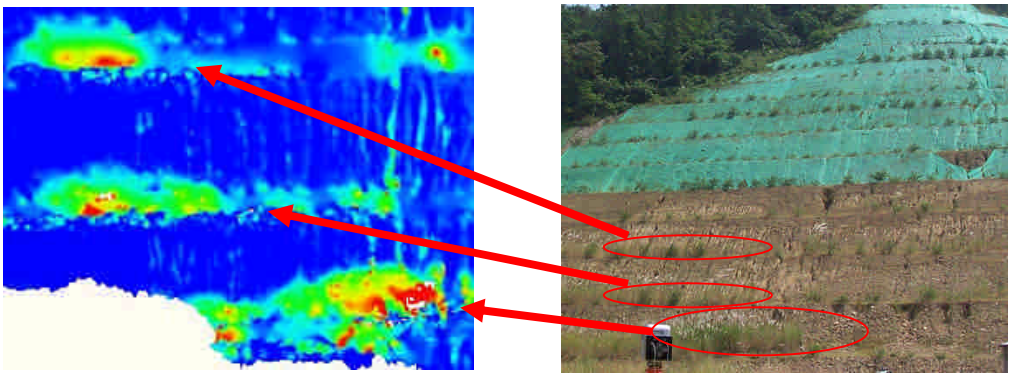

Fig. 15 Possible wrong judgment on surface variation due to weeds growing.

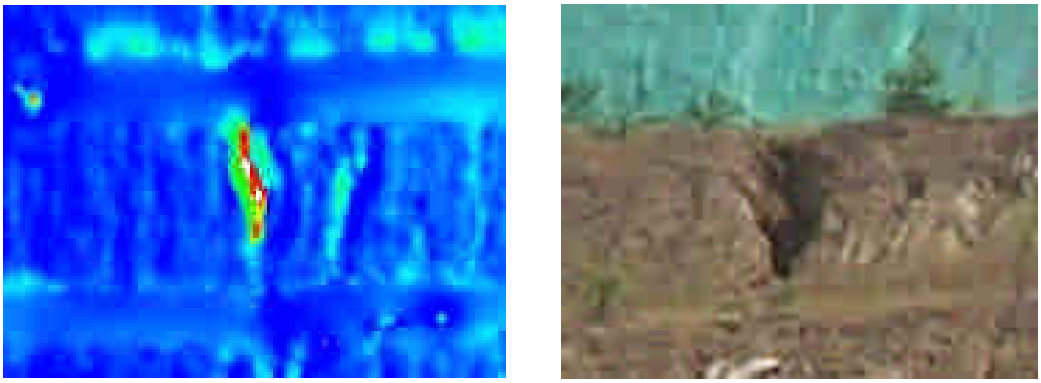

Fig. 16 The sliding area revealed by the second scanning and overlapping (left); the site photo of the sliding area.

5. Conclusions and suggestions

This study applied ground-based LiDAR to obtained accurate 3D coordinates of the topography of a slope. Terrain changes and deformation of the slope were analyzed, including calculation of the volumes of accumulation and depletion zones that occurred during the two measurements. This study proves that application of the technique on slope/landslide monitoring is feasible. The operations are easy and timing saving for a complete measurement and comparison. Also, the study shows that there is no translational system error between the two measurements. We can further apply 3D scanning technology for slope for understanding long-term creep tendency, detection of extent of landslide and prediction/warning of future sliding.

From the analysis of the scanned data, it shows that the position of 3D laser scanner will affect the data interpretation among different measurements, especially at those with larger undulate areas. Therefore, installation of a fixed base-plate for scanning station is suggested for the 3D scanner to maintain a same position for measurements preformed on different dates. The

analysis results of this study can indicate the position of changes and deformations of a slope. However, the changes and deformation should be verified with site photos to avoid making wrong judgment.

6. References

[1] Boehler, W., G.Heinz, A. Marbs, 2001. The Potential of Non-contact Close Range Laser Scanners for Cultural Heritage Recording, Proceedings of CIPA International Symposium, Potsdam, Germany.

[2] Gordon, Stuart, Derek Lichti and Mike Stewart, 2001. Application of a High-Resolution Ground-baesd Laser Scanner for Deformation Measurements, 19 – 22 March 2001 Orange, California, USA 23

[3] Zheng-yi Feng, Jia-Chi Liang, Tzong-Jiang Wu 2006.Three-dimensional Laser Scanning and Stability Analysis of Slopes, Journal of Soil and Water Conservation, Vol.38, No.2, pp.117-128 (in Chinese).